International Journal of Mass Spectrometry 304 (2011) 165–171

Contents lists available at ScienceDirect

International Journal of Mass Spectrometry

journal homepage: www.elsevier.com/locate/ijms

Alkali cation regulation of the dissociation and hydrobromination of a deprotonated trideoxynucleotide

Janna Anichina[a], Andreas Krapp[b], Einar Uggerud[b], Diethard K. Bohme[a,*]

[a] Department of Chemistry and Centre for Research in Mass Spectrometry, York University, 4700 Keele Street, Toronto, Ontario, Canada M3J 1P3
[b] Massespektrometrilaboratoriet og Senter for teoretisk og beregningsbasert kjemi (CTCC), Kjemisk institutt, Universitetet i Oslo, Postboks 1033, N-0315 Blindern, Oslo, Norway

ARTICLE INFO

Article history:
Received 29 March 2010
Received in revised form 19 July 2010
Accepted 2 August 2010
Available online 10 August 2010

Keywords:
Proton
Na^+
Trideoxycytoside CCC
Hydrogen bromide
Gas-phase stability
Gas-phase reactivity

ABSTRACT

Mass spectrometric experiments have been performed to compare the gas-phase stability and reactivity of the protonated and alkaliated forms of the trideoxycytoside dianion $(CCC–2H)^{2-}$, viz. $(CCC–H)^-$ and $[M(CCC–2H)]^-$, respectively, M = Li, Na, K, Rb, Cs. Collision-induced dissociation (CID) measurements exhibit a much-enhanced stability against the loss of neutral cytosine for the metallocomplexes compared to $(CCC–H)^-$. Also, $[Na(CCC–2H)]^-$ was observed to sequentially add 5 molecules of hydrogen bromide similar to the observed HBr addition to the $(CCC–2H)^{2-}$ dianion, but different from that observed for the $(CCC–H)^-$ monoanion. Quantum chemical calculations (RI-MP2) provide structural and energetic results for the sodiation and hydrobromination of the anions that are consistent with experiments and shed light on the ability of M^+ to influence the properties of oligonucleotides, including DNA.

1. Introduction

Understanding the mechanisms of DNA interactions with environmental contaminants is crucial in the assessment of the toxicological risks imposed by these substances since carcinogenicity is directly linked to DNA damage [1]. One of the classes of known environmental contaminants is hydrogen halides [2]. Hydrogen halides enter the environment mostly as the result of industrial activity. Hazardous effects of HCl, HBr, etc. generally are well established; however the primary molecular targets of these compounds need to be clarified. Interactions of DNA with hydrogen bromide, one of the major components in combustion mixtures, may serve as a model of DNA damage that arises from exposure to other environmental chemicals [3].

Our previous study of the physico-chemical properties of DNA ions addressed gas-phase reactivity of HBr with mono and dianions of a trideoxycytocide – CCC [4]. The importance of this particular sequence emerges from the fact that trideoxynucleotides are the shortest sequences that are called codons for their ability to code for a particular amino acid that will be synthesized upon transcription. CCC represents an example of a proline codon, one of three nucleotides in DNA that encodes proline amino acid. Even though such a model system lacks the complexity of cellular DNA, it should provide insights into the major sites of HBr reactivity on DNA (nucleobases, deoxyribose moieties, phosphate groups).

In the present study we address the influence of DNA metallocomplexation upon HBr reactivity towards nucleic acids. The negatively charged DNA molecule *in vivo* is well known to be neutralized by nearby counter cations, mostly alkaline and alkaline earth ions [5]. However, little is known about the influence of metal ions on the properties of oligonucleotides in a pristine gas-phase environment, such as their intrinsic chemical stability and reactivity in a solvent-free medium. Gas-phase interactions of alkali monocations with nucleobases were studied in detail previously by Rodgers and Armentrout [6]. Stano et al. studied the influence of sodium on the gas-phase fragmentation of deoxynucleotides [7].

Recently, we have coupled an electrospray ionization source to a selected ion flow tube/triple quadrupole (SIFT/QqQ) mass spectrometer that allows the quantitative measurement of rate coefficients and product distributions for gas-phase chemical reactions of deprotonated oligodeoxynucleotide anions with gases or vapours of liquids [8]. This new instrument, along with a commercial ESI triple quadrupole mass spectrometer, has been employed successfully in the exploration of the gas-phase structures, stabilities and reactivities of deprotonated oligonucleotides [4,8,9]. Our previous experiments have shown that reactivity with hydrogen bromide is a useful probe of the gas-phase acidity of oligonucleotides and their number of basic sites generally.

* Corresponding author. Tel.: +1 416 736 2100; fax: +1 416 736 5936x66188.
E-mail address: dkbohme@yorku.ca (D.K. Bohme).

1387-3806/$ – see front matter © 2010 Elsevier B.V. All rights reserved.
doi:10.1016/j.ijms.2010.08.001

Here we report computational results for the alkali metal complexes with CCC dianion, $[M(CCC–2H)]^-$, as well as experimental results for the stability of these anions against collision-induced dissociation (CID) and the gas-phase reactions of $[Na(CCC–2H)]^-$ with hydrogen bromide.

2. Experimental

Electrospray ionization MS data were acquired in the negative ion mode using an API 2000 (MDS-SCIEX, Concord, ON, Canada) triple quadrupole (Q1q2Q3) mass spectrometer equipped with a "TurboIon Spray" ion source. Experiments were performed at an ionspray voltage of −5500 V, a ring-electrode potential of −300 V (used for ion beam confinement). N_2 was used as a curtain gas at a setting of 70 kPa, and air was used as nebulizer gas at a flow rate of 8 L min^{-1}. Samples were directly infused into the electrospray source at a flow rate of 3 μL min^{-1}. MS/MS experiments were carried out in the product ion and multiple reaction monitoring (MRM) modes at the declustering potential of −150 V with N_2 as collision gas at a pressure estimated to be about 400 Pa (viz. multicollision conditions). The collision-offset voltage (the potential difference between the quadrupole entrance lens (q_0) and the collision cell quadrupole (q_2)), which nominally gives the laboratory frame collision voltage, was adjusted between −1 and −130 V at 1 V intervals. Space charge and contact potentials, field penetration, and field distortion can influence the actual collision energy, but were not taken into account. Product ion spectra were then obtained by scanning Q_3 over the range m/z 10–1800. The interquadrupole lens potentials and the float potential of the resolving quadrupole Q_3 were linked to the q_2 potential to maintain proper transmission through Q_3. The onset energy of a particular primary dissociation was determined by extrapolating the steepest slope of a plot of the sum of the relative intensities of the primary dissociation product and all its second and higher generation fragments [4]. The precision of the onset energy is taken to be one standard deviation from the mean onset voltage value obtained in several (four or more) repeated experiments. In the preparation of sample solutions, CCC was dissolved in an 80:20 (%) water:methanol mixture at a concentration of 10 μM and a five-fold molar excess of the alkali chloride was added to induce the metallocomplexation. HPLC degree methanol and Millipore (18.2 mΩ) water were used to prepare the solvent mixtures. CH_3OD purchased from Sigma–Aldrich and heavy water of 99.75% purity were utilized for the preparation of the solvent mixture in H/D exchange in solution.

All of the measurements of the gas-phase chemical reactivity of $[Na(CCC–2H)]^-$ anion with HBr were obtained using the ESI/SIFT/QqQ tandem mass spectrometer [8]. Ions were selected according to their m/z value with a quadrupole mass filter and injected through an aspirator-like interface into the flow tube, continuously flushed with helium buffer gas at 47 ± 1 Pa and 295 ± 2 K. The ions undergo approximately 105 collisions with He atoms prior to entering the reaction region of the flow tube and this ensures that they have reached a translational temperature equal to the tube temperature of 295 ± 2 K prior to reacting with HBr. HBr vapour was diluted in He gas in a reservoir system and introduced via a needle valve into the reaction region of the flow tube. Downstream of the reaction region, a second quadrupole mass filter was used to monitor the intensities of reactant and product ions as a function of the flow of HBr. Rate coefficients for the primary reactions of the reactant ions with HBr are determined with an uncertainty of ∼30% from the rate of decay of the reactant ion intensity assuming pseudo-first-order kinetics. HBr (99.0%) was obtained from Sigma–Aldrich Co. and used without further purification.

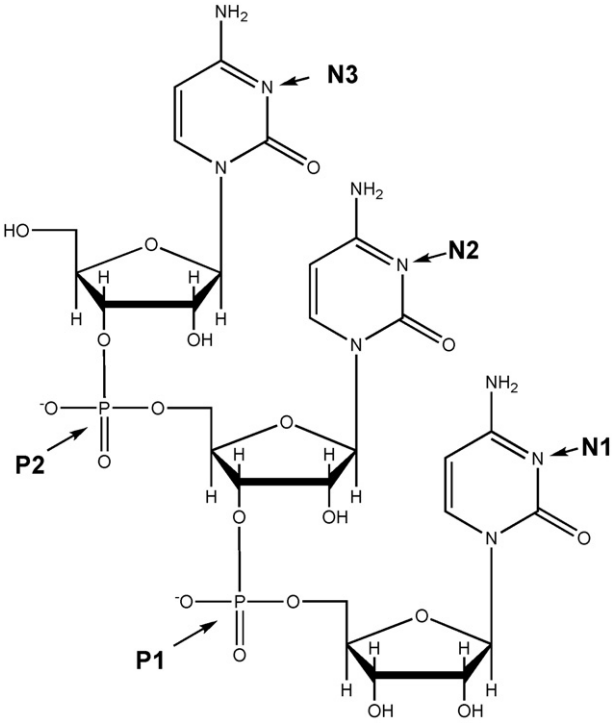

Fig. 1. Scheme of the structure of the $(CCC–2H)^{2-}$ dianion.

3. Computational procedure

The search for the most stable structure of the sodium complex of $(CCC–2H)^{2-}$ was performed following a procedure outlined previously [4]. The lowest energy conformers of both $Na(DMPHOS)_2^-$ and $[Na(CCC–2H)]^{2-}$ were subjected to final and full geometry optimization with RI-BP-86/SVP, as implemented in the TURBOMOLE package (DMPHOS = dimethylphosphate) [10–14]. Each of the lowest energy RI-BP-86/SVP configurations was finally subjected to single point calculation utilizing RI-MP2/TZVPP [15] again taking advantage of the TURBOMOLE code. Structures of mono- and di-adducts with HBr were optimized starting with the $[Na(CCC–2H)]^{2-}$ geometry. In addition, calculations were also performed for the dimethylphosphate ester $(DMPHOS)^-$ as a model of the phosphate group, and its dimer with the sodium cation, with B3LYP/6-31G* using Gaussian 03. Geometries of the complexes with the other alkali atoms were conducted by substituting sodium in the above-mentioned complexes with the each of the other alkali metals with subsequent geometry optimization.

4. Results and discussion

4.1. Pathways of collision-induced dissociation

In order to compare the fragmentation patterns and relative gas-phase stabilities of the protonated CCC dianion (Fig. 1) and the corresponding alkaliated anions, we first electrosprayed solutions containing the alkali chloride and trideoxycytoside to form the desired complexes. Fig. 2 shows examples of Enhanced Resolution (ER) scans of the ion of interest with M = Na. Such scans were routinely obtained at different values of the cone voltage (Declustering Potential, DP) (Fig. 2) in order to ensure the proper assignment of the charge and composition of peaks due to ions of interest. The top spectrum in Fig. 2 (DP = −30 V) indicates the presence of an isobaric mixture at m/z of 826, nominally corresponding to $[Na(CCC–2H)]^-$. The 0.5 amu spacing between 826.6 and 827.1 provides evidence for the presence of a doubly charged species, however the over-

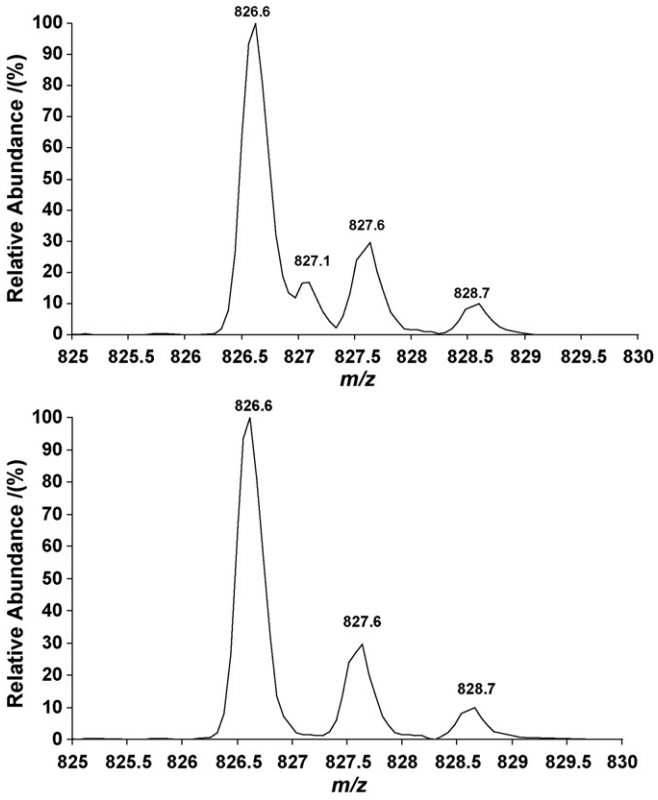

Fig. 2. Enhanced resolution spectra of m/z 826 $[Na(CCC–2H)]^-$ at declustering potentials of −30 V (top) and −150 V (bottom), respectively.

all isotopic distribution indicates that the mixture consists of two complex anions: $[Na(CCC–2H)]^-$ and $[Na_2(CCC)_2–4H]^{2-}$. The theoretical intensity of m/z 827.1 would account for 72% of the height of m/z 826.6, provided that only $[Na_2(CCC)_2–4H]^{2-}$ is present. But the experimental data clearly show that this is not the case. The isotopic ratio of the peaks spaced by 1 amu is very close to the theoretical isotopic distribution of $[Na(CCC–2H)]^-$. Interestingly, an increase in the DP from −30 to −150 V resulted in a complete disappearance of the peaks spaced by 0.5 amu indicating the occurrence of the dissociation of the doubly sodiated dianion of the CCC duplex. In order to avoid possible complications in the interpretation of the data, we performed all MS/MS and MRM measurements at a DP of −150 V.

CID profiles for $[M(CCC–2H)]^-$ with M = H, Li, Na, K, Rb and Cs are displayed in the different panels of Fig. 3. These profiles clearly show that the dissociation of all monoanions proceeds in a similar fashion. The initial loss of the neutral cytosine nucleobase is followed by the energetically only slightly more demanding loss of the adjacent furfuryl alcohol. This observation indicates that the initial loss of cytosine takes place at the end of the monoanions rather than in the middle of the oligonucleotide. However, the alkaliated forms exhibit greater stability against dissociation than the protonated analogue. This can be inferred from the observed dependence on the collision energy listed in Table 1. The data were obtained under similar collision cell conditions. However, these conditions do not ensure a strictly single collision regime, so the centre-of-mass energies in Table 1 do not allow for absolute threshold determinations. Nevertheless, the most stable complex appears to be that of the lithium monocation while Na(I), K(I), Cs(I) and Rb(I) exhibit similar energetics of CID that indicate only a slightly lower stability. We hypothesize that the higher charge localization on smaller metal ions results in an enhanced electrostatic interaction with various sites on the nucleic acid and therefore a more stable structure. The

Table 1
Onset voltages (OV), and corresponding center-of-mass onset energies (E_{CM}, eV) for $[M(CCC–2H)]^-$ (M = H–Cs) colliding on N_2.

M^+	OV, V	E_{CM}, eV
H	(23.6 ± 0.4)	0.8
Li	(36.6 ± 0.4)	1.2
Na	(34.4 ± 0.3)	1.1
K	(35.6 ± 0.4)	1.1
Rb	(33.9 ± 0.5)	1.0
Cs	(36.4 ± 0.4)	1.1

much lower gas-phase stability of the $[H(CCC–2H]^-$ species may be explained by the labile acidic proton that is easily transferred to the cytosine constituent of the CCC anion to form a stable neutral molecule, cytosine.

As we have demonstrated previously [4], the loss of one neutral cytosine molecule from the $(CCC–H)^-$ ion is accompanied by the transfer of the most acidic proton, residing on the neutral phosphate group to the departing nucleobase. This was inferred from MS/MS experiments utilizing the partially deuterated analog of $(CCC–H)^-$ [4]. The alkali cation adducts of trideoxycytoside do not posses such a proton on any of their phosphate groups. Therefore, a different mechanism must be involved in the loss of a neutral nucleobase. The aforementioned higher onset for the same type of dissociation further implies such a difference. CID experiments performed with the corresponding partially deuterated sodium complex demonstrated that a proton, not a deuteron is transferred to the departing nucleobase in the initial dissociation event (Fig. 4). H/D exchange experiments performed in solution indicated that there are nine exchangeable hydrogens in the structure of the singly deprotonated trideoxycytoside: a proton on one the phosphates, two of the terminal hydroxyl groups and six of the primary amino groups of the cytosine nucleobases. Our previous measurements [4] indicate that upon CID of the deuterated $(CCC–D)^-$ instead of the neutral loss of 111 amu (that corresponds to the molecular mass of a cytosine molecule) we observed a neutral loss of 114 amu that nominally gives the molecular mass of a cytosine molecule in which three amino hydrogens are replaced by deuterons [4]. The sodium complex of the trideoxycytoside that was electrosprayed from the solution prepared in 20:80 CH_3OD:D_2O exhibited the loss of 113 amu with the formation of m/z 721 instead of 114 and this provides evidence for the difference in the mechanism of the elimination of a neutral cytosine from $(CCC–H)^-$ compared to $[Na(CCC–2H)]^-$. A likely mechanism for the cytosine elimination from $[Na(CCC–2H)]^-$ involves the transfer of a proton from the fourth carbon of the neighbouring terminal deoxyribose ring (either 5′ or 3′), a proposition that is strengthened by the observed subsequent loss of the furfuryl alcohol. The peak at m/z 622 in Fig. 4 corresponds to the loss of furfuryl alcohol from m/z 721, while that at m/z 608 reflects the loss of two deuterated cytosines (neutral loss of 266 from the parent ion). m/z 608 is a secondary generation product ion of the parent m/z 721 that corresponds to the loss of a deuterated cytosine. To confirm the origins of the higher order dissociation daughter ions we performed CID measurements with the in-source generated primary and secondary dissociation products (data is not shown) such as m/z 721, 622 and 608 as well as the neutral loss scans for the molecular masses of 113. On the basis of these measurements we can unambiguously identify the formation of the $^dw_1^-$ ion at m/z 309 as the result of the fragmentation of m/z 721 and 622.

4.2. Reactions of $[Na(CCC–2H)]^-$ with hydrogen bromide

The monoanion $[Na(CCC–2H)]^-$ was found to react with HBr by sequential hydrobromination (see Fig. 5). The primary hydrobromination reaction was observed to be fast and proceed

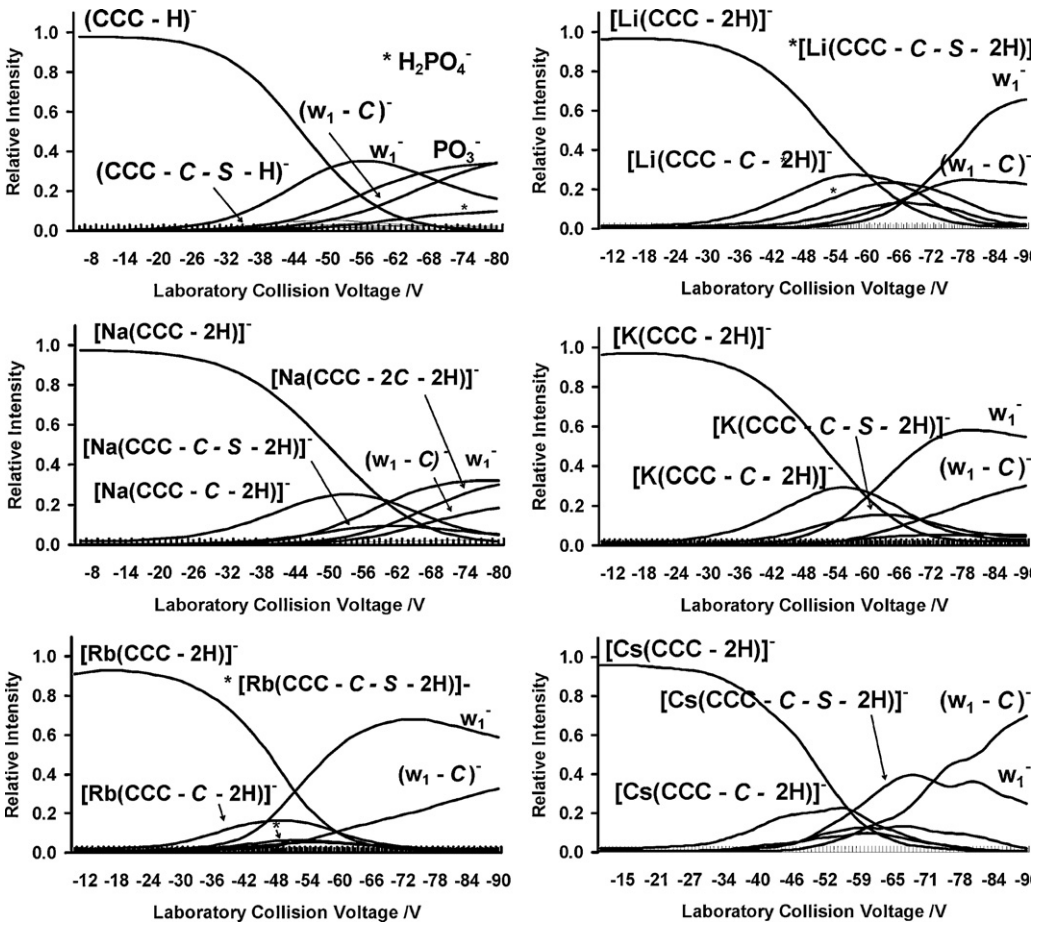

Fig. 3. CID profiles for $[M(CCC–2H)]^-$ with M = H, Li, Na, K, Rb, Cs. Product ions with intensities less than 0.5 are not shown. S designates furfuryl alcohol. The declustering potential was −150 V.

with an effective bimolecular rate coefficient $k = 7.0 \times 10^{-10}$ cm^3 molecule^{-1} s^{-1} and the next 4 HBr molecules add in rapid succession. Most likely, the additions proceed by termolecular collisional stabilization with He acting as the third body, although bimolecular radiative stabilization cannot be ruled out since the measurements were not conducted as a function of total pressure. The observed reactivity of $[Na(CCC–2H)]^-$ raises a number of questions, especially regarding the sites of the molecule that are involved in HBr bonding. Our previous investigation of the reactions of $(CCC–2H)^{2-}$ and $(CCC–H)^-$ with HBr [4] showed that the doubly deprotonated CCC reacts with hydrogen bromide both by addition (78%) and by

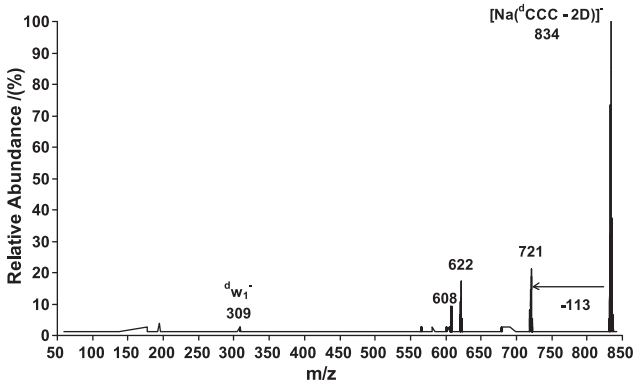

Fig. 4. MS/MS spectrum of the deuterated complex of Na^+ with trideoxycytoside acquired at the laboratory collision voltage of 35 V. The declustering potential was −150 V.

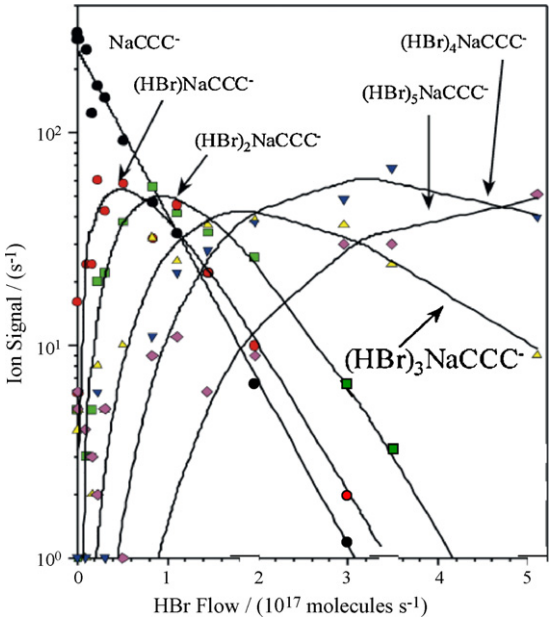

Fig. 5. Kinetic reaction profile obtained by ESI/SIFT/QqQ for subsequent hydrobromination of $[Na(CCC–2H)]^{2-}$ with HBr in a helium buffer gas at 47 ± 1 Pa and 292 K $[Na(CCC–2H)]^{2-}$ is abbreviated to $NaCCC^-$.

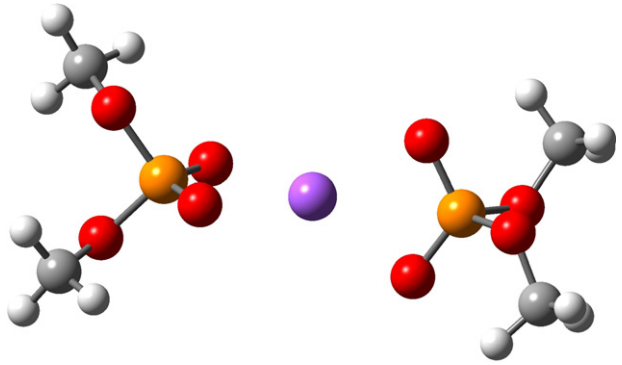

Fig. 6. Minimum energy structure of $Na(DMPHOS)_2^-$. Colour code: Na – pink, P – orange, O – red, C – grey and H – white (For interpretation of the references to colour in this figure legend, the reader is referred to the web version of this article.).

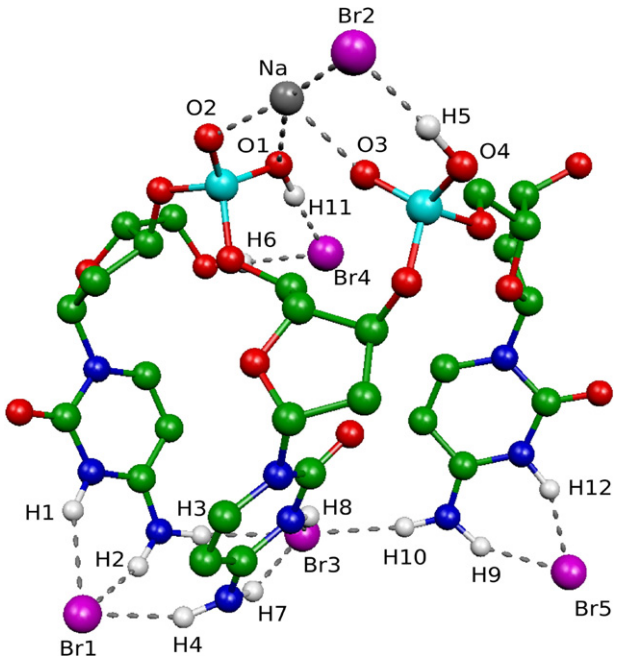

Fig. 7. Optimized (RI-BP86/SVP) structure of $Na(CCC–2H)^-$. Selected bond lengths (in Å): Na–O1 = 2.434, Na–O2 = 2.359, Na–O3 = 2.591, Na–O4 = 2.292.

proton transfer (22%), while the singly deprotonated CCC reacts only by HBr addition and not by proton transfer. These observations are consistent with the computed proton affinities of $(CCC–2H)^{2-}$ and $(CCC–H)^-$ anions that bracket the known proton affinity of Br^- [4]. The observation that HBr does not protonate $[Na(CCC–2H)]^-$ may therefore indicate a value of the proton affinity (PA) that also is lower than that of Br^-, although we realize that reaction kinetic factors may complicate this simple interpretation.

The observed addition of 5 HBr molecules to the $[Na(CCC–2H)]^-$ anion was initially surprising since the Na^+ might be expected to shield one of the two negatively charged phosphate groups of $(CCC–2H)^{2-}$ from attack by HBr, in analogy with $(CCC–H)^-$. However, this turned out not to be the case, a finding which will be discussed in more detail in the following section.

4.3. Results of computations

In order to mimic the interaction between the phosphate groups and Na^+, the structure of the sodium complex with two dimethylphosphate esters $(DMPHOS)^-$, mimicking the two phosphate groups in CCC) was computed first. The computed minimum energy structure is shown in Fig. 6.

RI-MP2 calculations using this dimethylphosphate ester mode indicate that the sodium ion affinity is 790 kJ mol^{-1}. The corresponding proton affinity is 1404 kJ mol^{-1}. Table 2 shows the corresponding affinities of all alkali metals to the dianion of CCC. On the other hand, binding the Na(DMPHOS) complex to a second dimethylphosphate ester to give $Na(DMPHOS)_2^-$, adds extra 225 kJ mol^{-1} to the binding energy. The computed binding energy is significantly higher than the analogous dimerization energy upon formation of $H(DMPHOS)^{2-}$, which is 127 kJ mol^{-1} [4]. The sodium ion is equidistant from the four oxygen atoms (2.38 Å) and forms a tetrahedral complex (Fig. 6).

Inclusion of a sodium cation into $(CCC–2H)^{2-}$ gives rise to the $[Na(CCC–2H)]^-$ ion presented in Fig. 7. Several geometric and energetic features of this structure are different from those of the idealized model of Fig. 6. Aside from the need to break two intramolecular hydrogen bonds present in $(CCC–2H)^{2-}$ in the incorporation of the sodium ion, severe conformational restrictions imposed by the phosphodiester backbone of the CCC dianion make the binding between two neighbouring DNA phosphate groups and a sodium ion less favourable than that found for the DMPHOS dimer. The sum of these factors leads to a computed sodium cation affinity of $(CCC–2H)^{2-}$ of 694 kJ mol^{-1} (RI-MP2), far lower than that of two $DMPHOS^-$ ions. In addition, we observe on an average 0.04 Å longer Na–O contacts, and note that the sodium has to find a less favourable position in $[Na(CCC–2H)]^-$ compared to a perfect relaxed tetrahedral environment in $Na(DMPHOS)_2^-$.

Analysis of Table 2 shows that the periodic trend in alkali metal binding is in good accord with an electrostatic binding model, since the $DMPHOS^{2-}$ affinity decreases with increasing atomic number, and since there is excellent linear correlation with the inverse of the ionic radius (not illustrated here). We also note the affinity to the dianion of CCC is systematically lower, as for M = Na. As a matter of fact, alkali metal affinities of $[(CCC–2H)]^{2-}$, $[(DMPHOS)_2]^{2-}$, and hydride are strictly linearly correlated.

Semi-empirical calculations by Weigend and Häser [15] and Green-Church and Limbach [16] indicate that the two most basic sites of deprotonated monocytoside are the phosphate and N3 of the cytosine. On this basis, we identify five hydrogen bond acceptor sites for the doubly negatively charged $(CCC–2H)^{2-}$ to be the phosphate groups, of which there are two, and the N3 positions of the cytosines, of which there are three. Therefore, the experimental observation that $(CCC–2H)^{2-}$ adds 5 HBr molecules while $(CCC–H)^-$ with its single negatively charged phosphate group, adds only 4, may be rationalized in terms of the number of free basic sites available for hydrogen binding [17]. In qualitative terms, the fact that $[Na(CCC–2H)]^-$ still accommodates 5 HBr molecules could be explained by the assumption that the sodium ion is unable to block one basic site as effectively as the proton. Our finding above that the sodium cation is rather relatively weakly bonded to $(CCC–2H)^{2-}$ is in line with this idea. In order to put this on a more quantitative basis, we also performed calculations of HBr binding to $[Na(CCC–2H)]^-$ as well as to the $Na(DMPHOS)_2^-$ model system (Table 3).

Table 2
M^+ affinities in kJ mol^{-1} at MP2/TZVPP//BP86/TZVPP (electronic energies only).

M^+	$[(CCC–2H)]^{2-}$	$[(DMPHOS)_2]^{2-}$	H^-
Li	789.6	883.9	181.0
Na	693.9	789.9	161.9
K	610.7	699.7	138.2
Rb	588.4	669.4	132.2
Cs	565.1	641.0	127.5

Table 3
The *n*th HBr affinity of $Na(DMPHOS)_2^-$ in kJ mol^{-1} at 298 K (ZPC at the RI-BP86/SVP level).

n	*E* (RI-BP86/SVP)	*E* (RI-MP2/TZVPP)
1	108	117
2	108	112
3	39	29
4	41	32

Table 4
The *n*th HBr affinity of $[Na(CCC–2H)]^-$ in kJ mol^{-1} at 298 K (ZPC at the RI-BP86/SVP level).

n[a]	*E* (RI-BP86/SVP)	*E* (RI-MP2/TZVPP)
1	146	151
2	114	120
3	112	108
4	87	105
5	100	85

[a] Protonation sites: 1. Protonation at cytosine ($C_{5'}$ terminus). Protonation at phosphate closest to $C_{3'}$ terminus. 3. Protonation at central cytosine. 4. Protonation at phosphate closest to $C_{5'}$ terminus. 5. Protonation at cytosine ($C_{3'}$ terminus).

For $Na(DMPHOS)_2^-$ we estimate rather similar binding energies for the addition of the first and the second HBr molecules, while the third and the fourth are weakly bonded (Table 3). For $[Na(CCC–2H)]^-$ it is clear that binding to the five most basic sites is significant, in good agreement with the experimental observation (Table 4). Fig. 8 shows the optimized geometry of the $[Na(CCC–2H)]^-(HBr)_5$ adduct. It is interesting that all 5 HBr molecules partially dissociate by protolysis upon addition. Such partial heterolytic bond dissociation is expected for addition to a formally negatively charged phosphate site. The observation that ion pair formation also occurs upon addition to the formally neutral nitrogen atoms of the cytosines is perhaps more surprising but there is literature precedence. For example, addition of HBr to pyridine in the gas phase or in a cold matrix leads to pyridinium bromide, as demonstrated by infrared and microwave spectroscopy, as well as quantum chemical calculations [18,19]. It is also informative to notice the estimated order of the HBr affinity of the different sites. From the footnote of Table 4 it appears that the cytosines are equally, or even better hydrogen bond acceptor sites than the phosphates. It is therefore clear that the sodium cation partially screens the phosphate sites, but only ineffectively since despite the complexation with Na^+ the two negatively charged phosphate groups of $[Na(CCC–2H)]^-$ are still accessible to HBr attachment. It is noticeable that binding the first HBr to the N3 nitrogen atom of the C5′ terminus is more profitable than binding to any of the phosphates.

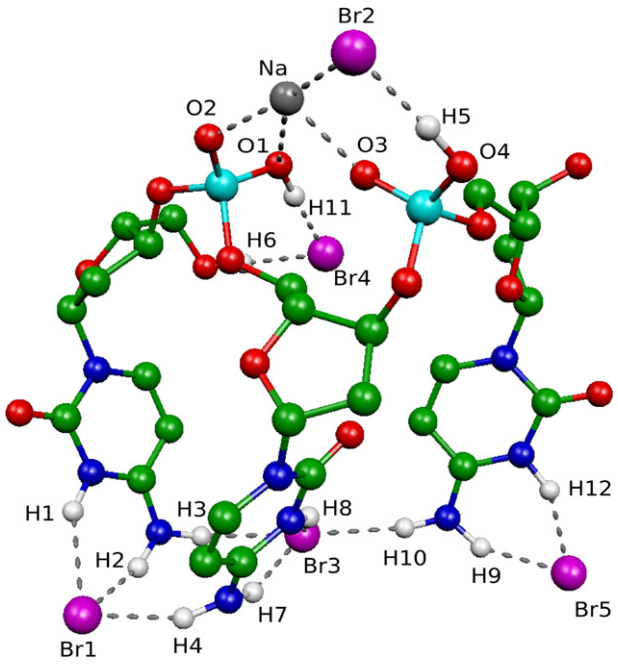

Fig. 8. Optimized (BP86/SVP) structure of $(NaCCC–2H)^-·5HBr$. Selected bond lengths (in Å): Na–O1 = 3.673, Na–O2 = 2.237, Na–O3 = 2.238, Na–O4 = 3.868, Na–Br2 = 2.735, H1–Br1 = 2.371, H2–Br1 = 2.288, H4–Br1 = 2.221, H3–Br3 = 2.406, H7–Br3 = 2.306, H8–Br3 = 2.352, H10–Br3 = 2.418, H11–Br4 = 2.010, H6–Br4 = 2.207, H9–Br5 = 2.163, H12–Br5 = 2.108.

The fact that no proton transfer occurs from HBr to $[Na(CCC–2H)]^-$ could in principle stem from an unfavourable kinetic factor. If proton transfer were only weakly exothermic the intermediate $[Na(CCC–2H)]^-$HBr complex would have a significant lifetime due to the combination of a moderate excess energy and a large number of internal degrees of freedom and could undergo one or several stabilizing collisions with bath gas molecules before dissociating into Br^- + [Na(CCC–H)]. To clarify this point, we computed the RI-MP2 proton affinities (PA) of the $Na(DMPHOS)_2^-$ model molecule and $[Na(CCC–2H)]^-$; they were found to be 1345 kJ mol^{-1} and 1323 kJ mol^{-1}, respectively. So the proton affinity of Br^- (experimental PA of 1354 kJ mol^{-1}, RI-MP2 value of 1356 kJ mol^{-1}) is somewhat higher than the computed proton affinity of $[Na(CCC–2H)]^-$ and this is fully consistent with a thermodynamic rather than a kinetic reason behind the experimental observation that no proton is transferred from HBr to $[Na(CCC–2H)]^-$. We also notice that PA{$[Na(CCC–2H)]^-$} = 1323 kJ mol^{-1} lies in-between PA{$[(CCC–2H)]^{2-}$} = 1562 kJ mol^{-1} and PA{$[(CCC–2H)]^-$} = 1206 kJ mol^{-1}. This result implies that the sodium ion is less effective than the proton in screening the most basic site (phosphate in both cases) making the sodiated form the more basic. However, the sodiated form is by far less basic than the dianion.

5. Final discussion and conclusion

On the basis of detailed mass spectrometric and computational quantum chemical data on the gas-phase properties of alkali trideoxynucleotide anions, $[M(CCC–2H)]^-$, a clear structural and mechanistic picture emerges. The tandem mass spectrometric measurements indicate a different mechanism for the loss of a neutral cytosine from $[M(CCC–2H)]^-$ (M = Li–Cs) compared to $[H(CCC–2H)]^-$. The apparent higher stability of the alkaliated complexes compared to the protonated is due to the latter having a more acidic hydrogen available to assist the dissociation. The CID profiles of the alkali metal ion complexes with cytosine trideoxycytoside also indicate a similar stability for these complexes with perhaps the Li complex being slightly more stable (Table 1). There may be a correlation with the computed M^+ affinities (Table 2) but the multiple collision conditions in the collision cell of the instrument do not allow this to be resolved.

The calculated minimum energy gas-phase structure of $[Na(CCC–2H)]^-$ shows how the alkali cation is somewhat asymmetrically bonded in a distorted tetrahedral ligand pocket formed by the two bidentate phosphate groups. This structure has a total of five basic sites available for hydrogen bonding, and in the case of M = Na the bond dissociation energies for successive addition of 5 hydrogen bromides have been calculated using different levels of theoretical computations [10–14,20]. These calculations provide a consistent rationale for the experimental observation that $[Na(CCC–2H)]^-$ accommodates up to 5 HBr molecules, forming the complex $(NaCCC–2H)^-·5HBr$. The proton affinity of $[Na(CCC–2H)]^-$ was calculated to be PA = 1323 kJ mol^{-1}, in-between $PA(CCC–2H)^{2-}$ and $PA(CCC–H)^-$.

These results show how the alkali ion regulates the acid/base properties of the twice deprotonated CCC to lie in-between that of the corresponding naked and protonated forms. Such perturbation of the inherent electronic structure by metal ions found in the biological environment are probably important to the function of oligonucleotides in particular and DNA in general. More work is needed to uncover the mechanisms of action of a range of other metal ions.

Acknowledgments

Continued financial support from the Natural Sciences and Engineering Research Council of Canada, the National Research Council, and MDS-SCIEX is greatly appreciated. As holder of a Canada Research Chair in Physical Chemistry, D.K.B. thanks the contributions of the Canada Research Chair Program to this research. A.K and E.U. are grateful to NOTUR for providing generous computational resources and the Norwegian Research Council for their Grant No. 179568/V30 to the Centre of Theoretical and Computational Chemistry through their Centre of Excellence program.

References

[1] M. Lynch, Regulatory DNA. The human genome, in: The Origins of Genome Architecture, Sinauer Associates, Sunderland, USA, 2007 (Chapter 3).
[2] J.V. Vincoli, Risk Management for Hazardous Chemicals. II, CRC Press, 1997.
[3] B.C. Levin, E.A. Kuligowski, Toxicology of fire and smoke, in: Inhalation Toxicology, Taylor and Francis, Boca Raton, USA, 2006 (Chapter 10).
[4] J. Anichina, S. Feil, E. Uggerud, D.K. Bohme, Structures, fragmentation and protonation of trideoxynucleotide CCC mono- and dianions, J. Am. Soc. Mass Spectrom. 19 (2008) 987–996.
[5] K. Aoki, Metal binding effects on nucleic acid structures, in: Comprehensive Supramolecular Chemistry, Pergamon, New York, USA, 1996.
[6] M.T. Rodgers, P.B. Armentrout, Noncovalent Interactions of nucleic acids bases (uracil, thymine and adenine) with alkali metal ions. Threshold collision-induced dissociation and theoretical studies, J. Am. Chem. Soc. 122 (2000) 8548–8558.
[7] M. Stano, H.D. Flosadottir, O. Ingolfsson, Rapid Commun. Mass Spectrom. 20 (2009) 3498–3502.
[8] G.K. Koyanagi, V.I. Baranov, S.D. Tanner, J. Anichina, M.J.Y. Jarvis, S. Feil, D.K. Bohme, A novel chemical reactor suited for studies of biophysical chemistry: construction and evaluation of a selected ion flow tube utilizing an electrospray ion source and a triple quadrupole detection system, Int. J. Mass Spectrom. 265 (2–3) (2007) 295–301.
[9] S. Feil, G.K. Koyanagi, J. Anichina, D.K. Bohme, Chemical stability and reactivity of deprotonated oligonucleotides (DNA) in the gas phase: protonation and solvation with hydrogen bromide, J. Phys. Chem. B 112 (2008) 10375–10381.
[10] K. Eichkorn, F. Weigend, O. Treutler, R. Ahlrichs, Auxiliary basis sets for main row atoms and transition metals and their use to approximate coulomb potentials. Theoretical chemistry accounts: theory, computation and modeling, Theor. Chim. Acta 97 (1997) 119–124.
[11] A. Schäfer, H. Horn, R. Ahlrichs, Fully optimized contracted Gaussian basis sets for atoms Li to Kr, J. Chem. Phys. 97 (1992) 2571–2577.
[12] A.D. Becke, Density-functional exchange-energy approximation with correct asymptotic behavior, Phys. Rev. A 38 (1988) 3098–4000.
[13] J.P. Perdew, Density-functional approximation for the correlation energy of the inhomogeneous electron gas, Phys. Rev. B 33 (1986) 8822–8824.
[14] F. Weigend, M. Haser, Patzelt, R. Ahlrichs, RI-MP2: optimized auxiliary basis sets and demonstration of efficiency, Chem. Phys. Lett. 294 (1998) 143–152.
[15] F. Weigend, M. Häser, RI-MP2: first derivatives and global consistency, Theor. Chim. Acta 97 (1997) 331–340.
[16] K.B. Green-Church, P.A. Limbach, Mononucleotide gas-phase proton affinities determined by the kinetic method, J. Am. Soc. Mass Spectrom. 11 (2000) 24–32.
[17] S. Pan, K. Verhoeven, J.K. Lee, Investigation of the initial fragmentation of oligodeoxynucleotides in a quadrupole ion trap: charge level-related base loss, J. Am. Soc. Mass Spectrom. 16 (2005) 1853–1865.
[18] K. Szczepaniak, P. Chabrier, W.B. Person, J.E. Del Bene, Ab initio theoretical and matrix isolation experimental studies of hydrogen bonding. IV. The HBr:pyridine complex, J. Mol. Struct. 436–437 (1997) 367–386.
[19] G.C. Cole, A.C. Legon, The nature of the complex formed between pyridine and hydrogen bromide in the gas phase: An experimental approach using rotational spectroscopy, J. Chem. Phys. 121 (2004) 10467–10473.
[20] M.J. Frisch, G.W. Trucks, H.B. Schlegel, G.E. Scuseria, M.A. Robb, J.R. Cheeseman, J. Montgomery, J.A.T. Vreven, K.N. Kudin, J.C. Burant, J.M. Millam, S.S. Iyengar, J. Tomasi, V. Barone, B. Mennucci, M. Cossi, G. Scalmani, N. Rega, G.A. Petersson, H. Nakatsuji, M. Hada, M. Ehara, K. Toyota, R. Fukuda, J. Hasegawa, M. Ishida, T. Nakajima, Y. Honda, O. Kitao, H. Nakai, M. Klene, X. Li, J.E. Knox, H.P. Hratchian, J.B. Cross, V. Bakken, C. Adamo, J. Jaramillo, R. Gomperts, R.E. Stratmann, O. Yazyev, A.J. Austin, R. Cammi, C. Pomelli, J.W. Ochterski, P.Y. Ayala, K. Morokuma, G.A. Voth, P. Salvador, J.J. Dannenberg, V.G. Zakrzewski, S. Dapprich, A.D. Daniels, M.C. Strain, O. Strain, O. Farkas, D.K. Malick, A.D. Rabuck, K. Raghavachari, J.B. Foresman, J.V. Ortiz, Q. Cui, A.G. Baboul, S. Clifford, J. Cioslowski, B.B. Stefanov, G. Liu, A. Liashenko, P. Piskorz, I. Komaromi, R.L. Martin, D.J. Fox, T. Keith, M.A. Al-Laham, C.Y. Peng, A. Nanayakkara, M. Challacombe, P.M.W. Gill, B. Johnson, W. Chen, M.W. Wong, C. Gonzalez, J.A. Pople, Gaussian03, Gaussian, Inc., Wallingford, CT, 2004.